Author Preprint Version – Paper published by Elsevier as:
T. Gernay, J.M. Franssen, Fire Safety J., 71 (2015), pp. 268-278

A plastic-damage model for concrete in fire: Applications in structural fire engineering

Thomas Gernay[a], Jean-Marc Franssen[b]

[a]The National Fund for Scientific Research F.R.S.-FNRS, Structural Engineering Department, Univ. of Liege, Ch. Des Chevreuils 1, 4000 Liege, Belgium, Thomas.Gernay@ulg.ac.be.

[b]Structural Engineering Dept, Univ. of Liege, Ch. Des Chevreuils 1, 4000 Liege, Belgium, JM.Franssen@ulg.ac.be.

Highlights:

- A constitutive model has been developed for concrete at high temperature.
- The model includes plasticity, damage and transient creep components.
- The model is used in advanced numerical analyses of concrete structures in fire.
- Standard values are used for the parameters of the model (no calibration required).
- The results illustrate the applicability and robustness of the concrete model.

ABSTRACT

The research aims at developing a new multiaxial constitutive model for concrete in the fire situation. In addition to validity at the material level, a crucial feature of a constitutive model is the applicability at the structural level; yet for concrete in fire there remains a serious lack of models combining reliability and robustness. The theoretical aspects and validation of the new model, which rely on a plastic-damage formulation, have been the subject of a former publication; they are briefly summarized here. This paper explores the capabilities of the concrete model for being used in a performance-based structural fire engineering framework. Several examples of numerical simulations by non-linear finite element method are discussed, with emphasis on practical applications that are demanding for the material model. In particular, it is shown that the simulations using the new concrete model succeed in capturing, at ambient temperature, the crack pattern in a plain concrete specimen and the influence of the loading path on reinforced concrete (RC) slabs. At high temperature, the presented applications include a RC slab subjected to furnace fire and a large-scale composite steel-concrete structure subjected to natural fire. In the numerical analyses, no parameter calibration was required on the particular concrete type, except for the uniaxial strengths and tensile crack energy which are to be defined case-by-case. The results illustrate the reliability and numerical robustness of the model. Also, they suggest that satisfactory prediction of structural behavior in fire can be obtained when no additional data is available on the specific properties of the particular concrete mix that is used in the project, as is often the case in practice, by using standard values of parameters.

Keywords: concrete; constitutive model; structural analysis; finite element analysis; fire.

1. Introduction

Advanced computational mechanics is a very powerful tool for investigating the behavior and the performance of structures subjected to fire. The last decades have seen significant advances in the development of these numerical methods. Owing to the increase in computing power and to the development of new concepts and theoretical tools, the capabilities of numerical methods have evolved from prescriptive evaluation of simple structural elements towards performance-based assessment of the fire behavior of complex structures. This evolution is necessary to improve understanding of the behavior of buildings in fires.

Since a few years, it has appeared that a significant new frontier in the development of the numerical methods lies in the proper modeling of the behavior of concrete material. Indeed, the numerical analysis of structures in fire requires reliable and robust temperature dependent constitutive models for the load-bearing materials used in the structure such as, for instance, steel and concrete. Despite the wide use of concrete material in civil engineering, modeling of concrete thermo-mechanical behavior remains a challenging issue for engineers. This is mainly due to the complexity of the concrete behavior characterization and to the severe requirements for material models raised by the development of performance-based design. Recurrent issues of concrete models are their lack of numerical robustness and their large number of parameters, both limiting the practical applicability of the models in real engineering projects.

Considering this situation, research efforts have been dedicated to the development of an advanced constitutive model for concrete in the fire situation which meets the requirements of structural fire engineers. At ambient temperature, research in computational mechanics has shown that the combination of continuum damage mechanics (CDM) with plasticity theory offers a very interesting theoretical framework for efficiently modeling the mechanical behavior of concrete material [1-9]. Yet, the development of concrete plastic-damage models at high temperature has been hardly treated in the literature. Nechnech et al. [10] proposed an interesting contribution which highlighted the interest of plastic-damage models for concrete at high temperature, but their model was not applied to practical examples of structural fire engineering, except for the very simple case of simply supported reinforced concrete beams. In the present work, it was decided to adopt the plastic-damage approach to develop a new multiaxial constitutive model for concrete in the fire situation. The model includes a number of original contributions, in particular regarding the modeling of transient creep phenomenon, the combination of the theories of elastoplasticity and damage at high temperature, the implementation of temperature-dependent relationships for the material parameters and the numerical integration of the constitutive laws in a finite element code. It has been developed for normal strength concrete. As the aim of the model is not to capture spalling, it should be used carefully when this could be an issue such as, for example, with some high-strength concretes. Above all, the model has been designed for use in real applications of structural fire engineering; therefore, emphasis has been put on combining an advanced constitutive model with a robust numerical implementation. Also for enabling practical usefulness, the model has been based on a limited number of physical parameters. Incorporation of all these features in a

model for concrete at high temperature contributes to fulfill the need for robust and reliable constitutive models in structural fire engineering.

It is noteworthy that advanced concrete models are needed for modeling of reinforced concrete structures in fire, both when these structures exhibit failure in concrete (e.g. cracking or crushing) or in other structural materials. Indeed, running a numerical analysis until failure may be demanding for the concrete material model whatever the structural failure mode. For instance, the development of tensile membrane action in composite slabs in fire has been extensively studied in the last years. Simulation of this behavior requires accommodating the several transitions between tension and compression in the concrete slab caused by thermal strains as well as by transition from a bending load transfer mode to a tensile membrane action mode. A robust and reliable concrete model is therefore needed, whether failure eventually occurs in the steel reinforcement, or by excess of compression in the concrete slab, which is a failure mode that is captured by the model.

The theoretical aspects of the model and its numerical implementation in finite element software are presented in another publication [11]; they are briefly summarized in Section 2. The former reference also includes the model validation based on experimental results on concrete samples at both ambient and elevated temperature. The present paper focuses on the model applicability at the structural level. The aim is to illustrate the capabilities of the concrete model in a performance-based framework; this is done by presenting numerical simulations of experimental tests on concrete structures, first at ambient temperatures then in the fire situation. Hence, Section 3 presents applications at ambient temperature and Section 4 addresses applications at high temperatures. These applications are used as a basis for discussing the model properties and capabilities. Demonstrating the practical applicability of a constitutive model developed at the material scale for structural analysis is an important step, although it is not so commonly addressed in the field. Many concrete models are developed with different objectives, for instance focusing on the proper modeling of the initiation and propagation of a single crack in a simple concrete member, or on the modelling of the hygro-thermo-mechanical mechanisms leading to spalling in heated concrete. Despite all their merits, these models are presently not intended to be used for more complex structures; or, at least, their usability to complex structures is not demonstrated. This usability requires specific properties in terms of numerical implementation and parameter identification. By addressing these issues, the present work has practical significance for researchers and for practitioners. It makes available a new model for concrete that is shown to be reliable and robust not only at the material scale, but also for the analysis of large structures in fire. It also gives essential information about the proper use of the material parameters for such applications as well as interpretation of the results. The model is available in finite element software and can be used for research and design projects.

2. Presentation of the model

2.1 Plastic-damage model

In the model, the total strain tensor $\underline{\underline{\varepsilon}}_{tot}$ is decomposed into elastic strain $\underline{\underline{\varepsilon}}_{el}$, plastic strain $\underline{\underline{\varepsilon}}_{p}$, free thermal strain $\underline{\underline{\varepsilon}}_{th}$ and transient creep strain $\underline{\underline{\varepsilon}}_{tr}$ according to Eq. (1) [10, 12].

The sum of the elastic strain and the plastic strain is referred to as instantaneous stress-related strain $\underline{\underline{\varepsilon}}_{\sigma}$.

$$\underline{\underline{\varepsilon}}_{tot} = \underline{\underline{\varepsilon}}_{el} + \underline{\underline{\varepsilon}}_{p} + \underline{\underline{\varepsilon}}_{th} + \underline{\underline{\varepsilon}}_{tr} \quad (1)$$

Considering that the plastic behavior occurs in the undamaged material, the characterization of plastic response can be formulated in the effective stress space following the classical elastoplastic theory. The elastic strain tensor is related to the effective stress tensor $\underline{\underline{\bar{\sigma}}}$ by means of the fourth-order isotropic linear-elastic stiffness tensor $\underline{\underline{\underline{\underline{C}}}}_0$, see Eq. (2).

$$\underline{\underline{\bar{\sigma}}} = \underline{\underline{\underline{\underline{C}}}}_0 : \underline{\underline{\varepsilon}}_{el} = \underline{\underline{\underline{\underline{C}}}}_0 : \left(\underline{\underline{\varepsilon}}_{\sigma} - \underline{\underline{\varepsilon}}_{p} \right) \quad (2)$$

Concrete exhibits damage mechanisms which are different in tension and in compression. In this model, a tensile damage scalar d_t and a compressive damage scalar d_c are adopted to capture the phenomenological effects induced by microcracking in concrete under tension and compression, respectively. Based on the work by Wu, et al. [6], these two damage scalars are applied to fourth-order projection tensors to lead to a fourth-order damage tensor $\underline{\underline{\underline{\underline{D}}}}$, which is employed to characterize the state of isotropic damage in concrete, see Eq. (3). This representation of the state of damage allows representing the effect of the tensile cracks closure on the material stiffness, when the stress state in the material changes from tension to compression (unilateral effect).

$$\underline{\underline{\sigma}} = \left(\underline{\underline{\underline{\underline{I}}}} - \underline{\underline{\underline{\underline{D}}}} \right) : \underline{\underline{\bar{\sigma}}} \quad (3)$$

A composite yield surface is used for capturing the concrete non-symmetrical behavior in tension and in compression; a Rankine yield criterion is used to limit the tensile stresses and a Drucker-Prager yield contour is used for compression. The equations of the composite yield surface are written in terms of effective stresses, see Eq. (4) where κ_t and κ_c are the tensile and compressive hardening parameters, respectively.

$$f_t \left(\underline{\underline{\bar{\sigma}}}, \kappa_t \right) \leq 0 \quad ; \quad f_c \left(\underline{\underline{\bar{\sigma}}}, \kappa_c \right) \leq 0 \quad (4)$$

By assumption, damage mechanism is coupled to plasticity in the model. Consequently, there is no specific threshold for damage and the evolution laws for tensile and compressive damage are driven by the accumulated plastic strains (in tension and compression, respectively). From a computational point of view, once convergence has been obtained in the plastic return mapping algorithm, update of the damage variables is thus an explicit calculation.

2.2 At high temperatures

For calculation of the free thermal strain, the relationship from Eurocode 2 [13] is adopted and generalized to multiaxial stress states using the assumption of isotropy.

The Explicit Transient Creep (ETC) Eurocode model, developed at University of Liege for uniaxial relationships [14, 15], is extended to the multiaxial case by assuming that the process of transient creep does not induce anisotropy [16], see Eq. (5).In this equation, $\dot{\underline{\underline{\varepsilon}}}_{tr}$

is the rate of transient creep strain, $\dot{\phi}(T)$ is the rate of the transient creep function [14], $\underline{\underline{\bar{\sigma}}}^{-}$ is the negative part of the effective stress tensor, $f_{c,20}$ is the compressive strength at 20°C and $\underline{\underline{\underline{\underline{H}}}}$ is the fourth order tensor proposed by de Borst and Peeters [16].

$$\underline{\underline{\dot{\varepsilon}}}_{tr} = \dot{\phi}(T)\, \underline{\underline{\underline{\underline{H}}}} : \frac{\underline{\underline{\bar{\sigma}}}^{-}}{f_{c,20}} \tag{5}$$

Concrete subjected to elevated temperatures exhibits thermo-mechanical degradation of its properties of strength and stiffness; this effect is taken into account through proper temperature dependency of the material parameters. The evolution laws of the parameters with temperature are taken from design codes such as Eurocode 2 [13], when available, or from experimental data published in the literature. Full details about the temperature-dependent relationships adopted for the material parameters are given in [11].

2.3 Identification of material parameters

The model contains ten material parameters listed in Table 1. These parameters can be obtained at ambient temperature by three basic tests: uniaxial compression test until failure comprising one unloading-reloading at peak stress, biaxial compression test until peak stress, and uniaxial tension test until failure. Each parameter in the model has a well identified effect on the computed response of the concrete, i.e. each parameter has a physical meaning. Based on experimental tests on concrete samples, it is possible to define standard values at ambient temperature for seven of these parameters [11]. These values have been derived for use with normal strength concrete, refer to [11] and [17] for validation. They can then be used in numerical simulations with normal strength concrete for a generic model, i.e. when no additional data is available on the specific properties of the particular concrete mix that is used in the project. However, they should not be used without further analysis for particular types of concrete such as light-weight or high strength concrete. Also note that, since the concrete model does not take into account spalling, it should be used carefully in applications that present significant risk of spalling, for instance due to the use of high strength mixes or young age concrete that contains high water content. The standard values, indicated in Table 1, have been used in the simulations presented in this paper.

For the three remaining parameters, nevertheless, a case-by-case analysis is necessary. The uniaxial compressive and tensile strengths must necessarily be specified as a function of the strength class of the concrete used in the project. The tensile crack energy density g_t is the ratio between the crack energy in tension $\bar{G}_t$ and the characteristic length l_c: $g_t = \bar{G}_t / l_c$. Evaluation of parameter g_t is complex because the characteristic length is a mesh-dependent parameter and because experimental results of the crack energy in tension at high temperatures show a significant scatter depending on the test specimens and test methods. A formula has been given by the CEB-FIB [18] for calculation of the crack energy in tension at ambient temperature, as a function of the mean compressive strength of concrete and the maximum size of aggregates. The objective when developing the CEB empirical formula was to use only parameters generally known to the designer. This formula has been found to agree with experimental results [19] and it has been used in the literature [5; 20]. For concrete used

in typical applications, it leads to a crack energy in tension that ranges between 50 and 150 N.m/m². Hence, the CEB formula has been adopted here for evaluating the crack energy in tension at ambient temperature. At high temperature, due to the dispersion of the data available in the literature, it is difficult to assess the evolution of this energy parameter. It is noted that this crack energy is related to the area under the tensile hardening function curve. As temperature increases, the tensile strength decreases; when the latter eventually becomes null, the crack energy is also reduced to zero. Therefore, for practical purpose, it was decided to assume the same temperature relationship for the crack energy in tension as for the tensile strength.

Table 1: Material parameters in the concrete model.

Parameter	Symbol	Units	Standard value at room temperature*
Poisson's ratio	ν	[−]	0.20
Compressive limit of elasticity	f_{c0}	[N/m²]	0.30 f_c
Biaxial compressive strength	f_b	[N/m²]	1.16 f_c
Peak stress strain	ε_{c1}	[−]	2.5 10^{-3}
Dilatancy parameter	α_g	[−]	0.25
Compressive dissipated energy	x_c	[−]	0.19
Compressive damage at peak stress	$\tilde{d}_c$	[−]	0.30
Uniaxial compressive strength	f_c	[N/m²]	(**)
Uniaxial tensile strength	f_t	[N/m²]	(**)
Tensile crack energy density	g_t	[N/m²]	(**)

(*) standard values of the parameters are proposed for modelling a generic concrete
(**) value varying depending on the particular concrete that is modeled

The characteristic length is used for regularization of the material constitutive law. This characteristic length is model-dependent as it depends on the chosen element type, element size, element shape and integration scheme [20]. Yet, a very simple formula has been proposed by Rots for biaxial case [21], based on the area of the element A_e and a modification factor α_l which is equal to 1 for quadratic elements and equal to $\sqrt{2}$ for linear elements: $l_c = \alpha_l \, . \, A_e^{1/2}$. This formula gives good approximation for most practical applications and has been adopted here.

2.4 Numerical implementation

The concrete model has been implemented [11] in the non linear numerical software SAFIR [22] developed at University of Liege for the simulation of the behavior of building structures in fire. The numerical analyses presented in this paper have been made using the software SAFIR.

3. Applications at ambient temperature

3.1 Mixed-mode fracture test

The first example deals with the simulation of the double-edge notched plain concrete specimen experimentally studied by Nooru-Mohamed [23]. This experiment has been used in the literature to test the efficiency of concrete constitutive models in biaxial stress states [24, 25]. The specimen, a 50 mm thick 200 x 200 mm square plate with two symmetrical notches of 25 mm by 5 mm, see Fig. 1, is subjected to a loading path combining shear and tension at ambient temperature. A shear force P_s of 5 kN is first applied through the frame along the left-hand side of the specimen above the notch; then, a tensile displacement d_n is applied at the top of the specimen until failure. The specimen is fixed at the bottom and along the right hand side below the notch. The loading is applied through a rigid loading frame, consisting of two loading plates at top and left upper parts that are glued to the specimen. The experimental crack pattern at the end of the test, as reported by Nooru-Mohamed, is also plotted in Fig. 1.

The numerical analysis is performed in plane stress condition. Square shell elements of 5 mm size are used, i.e. one single finite element layer is used on the width of the notch. The specimen is made of normal weight concrete. Measured compressive and tensile splitting strengths of respectively 38.4 N/mm² and 3.0 N/mm² have been reported [24]. For the used quadratic elements, the evaluation of the characteristic length using the simple formula proposed in [21] leads to: $l_c = \sqrt{A_e} = 5\,\text{mm}$. Considering a typical value of 75 N.m/m² for the crack energy in tension $\bar{G}_t$ at ambient temperature, this leads to a value of 15000 N/m² for the tensile crack energy density g_t. The values of the other material parameters used in the analysis are given in Table 1. No calibration of the parameters is thus required on the specimen studied here.

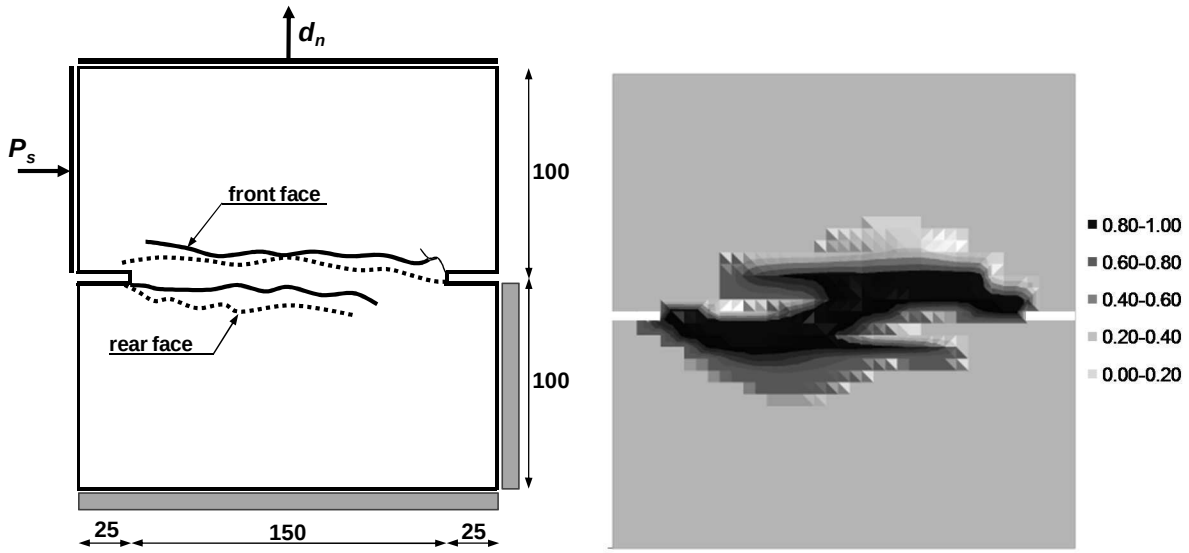

Fig. 1: Left – Geometry of the specimen and experimental crack pattern. Right – Distribution of tensile damage at the end of the numerical simulation.

The numerical simulation yields the distribution of tensile damage in the specimen, which can be compared at the failure stage to the experimental crack pattern (Fig. 1). The simulation captures the asymmetric crack propagation from the two notches and the

concentration of damage in a fracture zone in the center of the specimen. The simulation also yields the relationship between the tensile load and the average displacement in the vertical direction, see Fig. 2. The computed and measured results reasonably agree. In particular, the softening regime is well reproduced, which tends to validate the value used for the crack energy in tension.

In order to investigate the mesh sensitivity of the model, a new analysis is conducted using 2.5-mm size square shell elements, i.e. 2 finite element layers on the notch width. As the size of the square elements has been divided by 2 compared with the previous model, the characteristic length is also divided by 2, i.e. l_c = 2.5 mm. The obtained load-displacement relationship is plotted in Fig. 2. As can be seen, the peak tensile load is not dependent on the mesh size as long as the characteristic length is properly adjusted. However, a model with a mesh size of 2.5 mm and a characteristic length of 5 mm predicts a lower peak tensile load compared with the previous models. Note that one of the simulations using the finer mesh stopped in the softening regime due to numerical issues related to negative stiffness of the structure. The post-peak behavior appears to be slightly dependent on the mesh, even after regularization with the characteristic length. The analysis of the displacement evolution in the specimens shows that the specimen with a 5-mm size mesh and l_c = 5 mm and the specimen with a 2.5-mm size mesh and l_c = 2.5 mm present a similar displacement pattern at peak tensile load. Yet during softening, slight differences appear in the displacement pattern due to the refinement of the mesh.

This simulation shows that a load transfer mode, shear, that has not been used for the determination of the input parameters can nevertheless be addressed by the model.

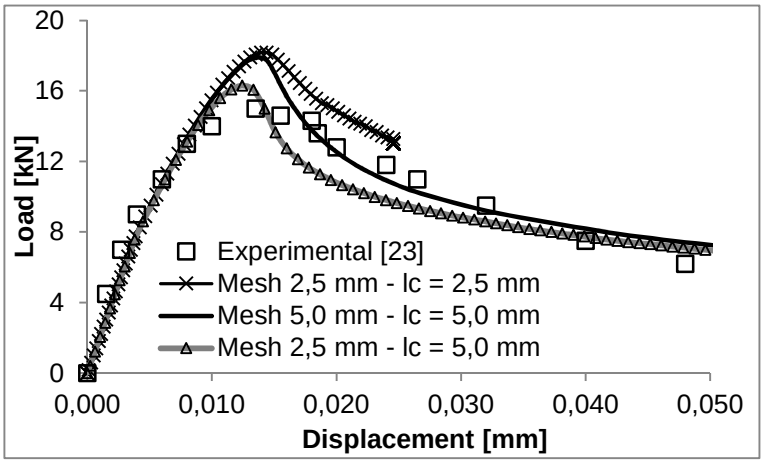

Fig. 2: Measured [23] and computed results for the mixed-mode fracture test on plain concrete.

3.2 RC slabs loaded in two directions

The second example deals with the simulation of an experimental test campaign performed at the University of Alberta [26] for investigating the behavior of reinforced concrete slabs subjected to combined in-plane and transversal loads at ambient temperature. For the ten simulated slabs, Table 2 gives the following data: length (L), width (l), average thickness (t), concrete compressive strength (f_c) and tensile strength (f_t), cover of the steel reinforcement from the compressive face for upper rebars (d'_x,d'_y) and lower rebars (d_x,d_y),

applied compressive in-plane loads (N_x, N_y) respectively in the X- and Y-directions, and applied transversal load (q_u). Fig. 3 shows a plan view of the two types of tested specimens, B and C, and the orientation of the axes. For all specimens, the area of reinforcement is 260 mm²/m at the top and at the bottom of the slab, in both directions, except for specimen C4 and C5 in which the reinforcement is doubled (520 mm²/m) respectively in the Y-direction and in the X-direction. The ultimate strength of the steel reinforcement is 620 N/mm², with the 0.2% offset yield at 450 N/mm². Specimens B1 and C1 were subjected to transversal loads only; the other specimens were tested under a combination of transversal loads and compressive in-plane loads.

The reinforced concrete slabs are modeled by means of shell finite elements with a square mesh of 0.06 m side. Due to the symmetry of the configurations, only a quarter of the slab is represented in the models, with symmetry boundary conditions. The support points in the experimental configuration illustrated in Fig. 3 are modeled by vertical supports. The steel rebars are considered in the shell elements. Following the model of Eurocode 2, the stress-mechanical strain relationship used for steel is non-linear until a strain of 0.02, with a horizontal plateau from 0.02 to 0.15 and a descending branch thereafter; unloading is plastic. The effective yield strength is taken equal to 620 N/mm².

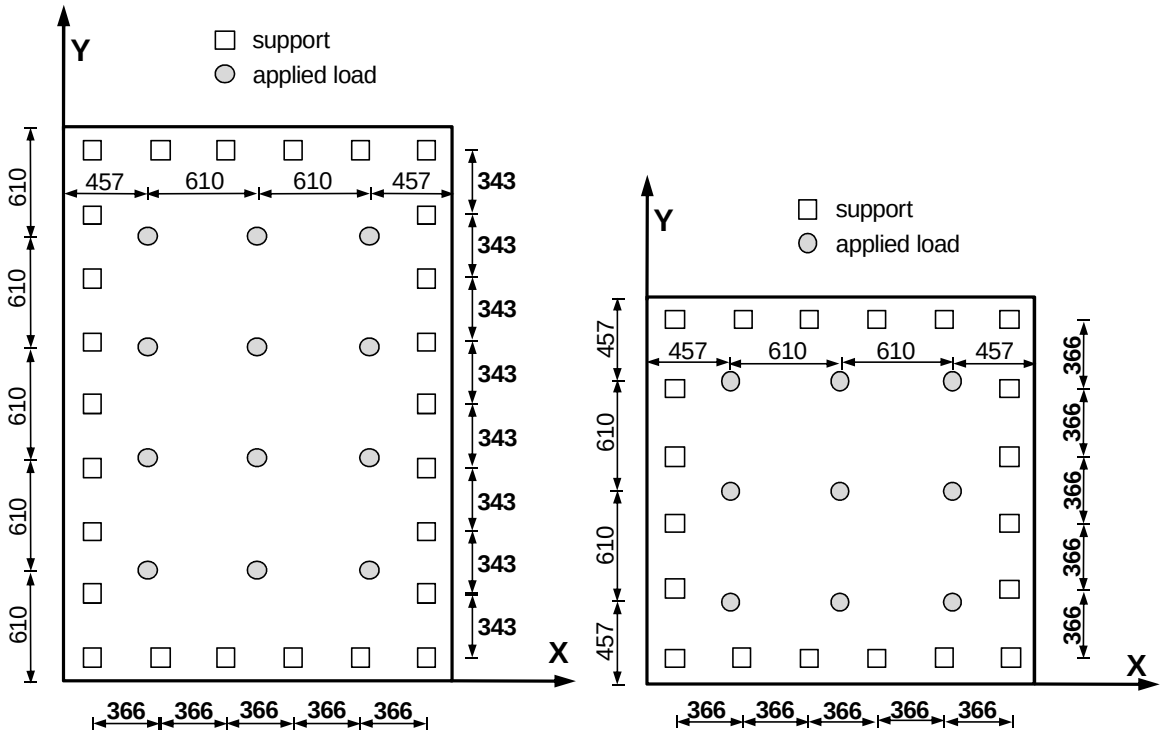

Fig. 3: Locations (in mm) of the lateral load and support points for series B (left) and series C (right).

The experimental results and the results of the numerical simulations are plotted in Fig. 4. For each test, the relationship is given between the applied transversal load in kN/m² and the central vertical deflection in mm. The numerical simulations succeed in capturing the initial stiffness of the structure in the different situations of combined in-plane and transversal loading. The maximum load is reasonably well predicted by the simulations. Application of

the load is simulated by increasing the load over time (force control) in the model; therefore failure of the structure is reached at the maximum load level and it is not possible to capture the post-peak behavior in the simulations. The simulation could not be conducted by increasing the displacement (deformation control) because an equal load must be applied simultaneously in different points. However in the experiments, the system was controlled near the maximum load to impose deflection increments and consequently the softening regime could be partly captured.

Table 2: Side dimensions, average measured thickness, concrete properties, average locations of top and bottom reinforcement from compressive face and maximum loads.

specimen	**B1**	**B2**	**B3**	**B4**	**C1**	**C2**	**C3**	**C4**	**C5**	**C6**
L [mm]	2745	2745	2745	2745	1829	1829	1829	1829	1829	1829
l [mm]	1829	1829	1829	1829	1829	1829	1829	1829	1829	1829
t [mm]	68.2	66.8	66.7	65.3	67.8	67.6	68.5	70.0	70.1	67.4
fc [MPa]	18.70	19.27	19.53	20.82	25.21	25.27	25.30	25.35	25.81	25.44
ft [MPa]	1.60	1.65	1.67	1.78	2.08	2.10	2.10	2.10	2.30	2.11
dx [mm]	55.0	53.5	53.3	50.3	56.8	57.6	57.6	58.5	52.5	56.1
d'x [mm]	22.3	20.5	20.2	19.7	21.9	19.7	19.9	20.9	14.4	18.1
dy [mm]	48.7	47.2	47.0	44.0	50.5	51.3	51.3	52.2	58.8	49.8
d'y [mm]	16.0	14.2	13.9	13.4	15.6	13.4	13.6	14.6	20.7	11.8
N_x [kN/m]	0.0	0.0	0.0	516.0	0.0	0.0	0.0	0.0	0.0	657.8
N_y [kN/m]	0.0	514.0	353.8	0.0	0.0	653.9	647.0	656.5	652.5	657.8
q_u [kN/m^2]	45.91	23.27	25.52	19.51	73.88	52.59	51.56	59.47	67.83	69.16

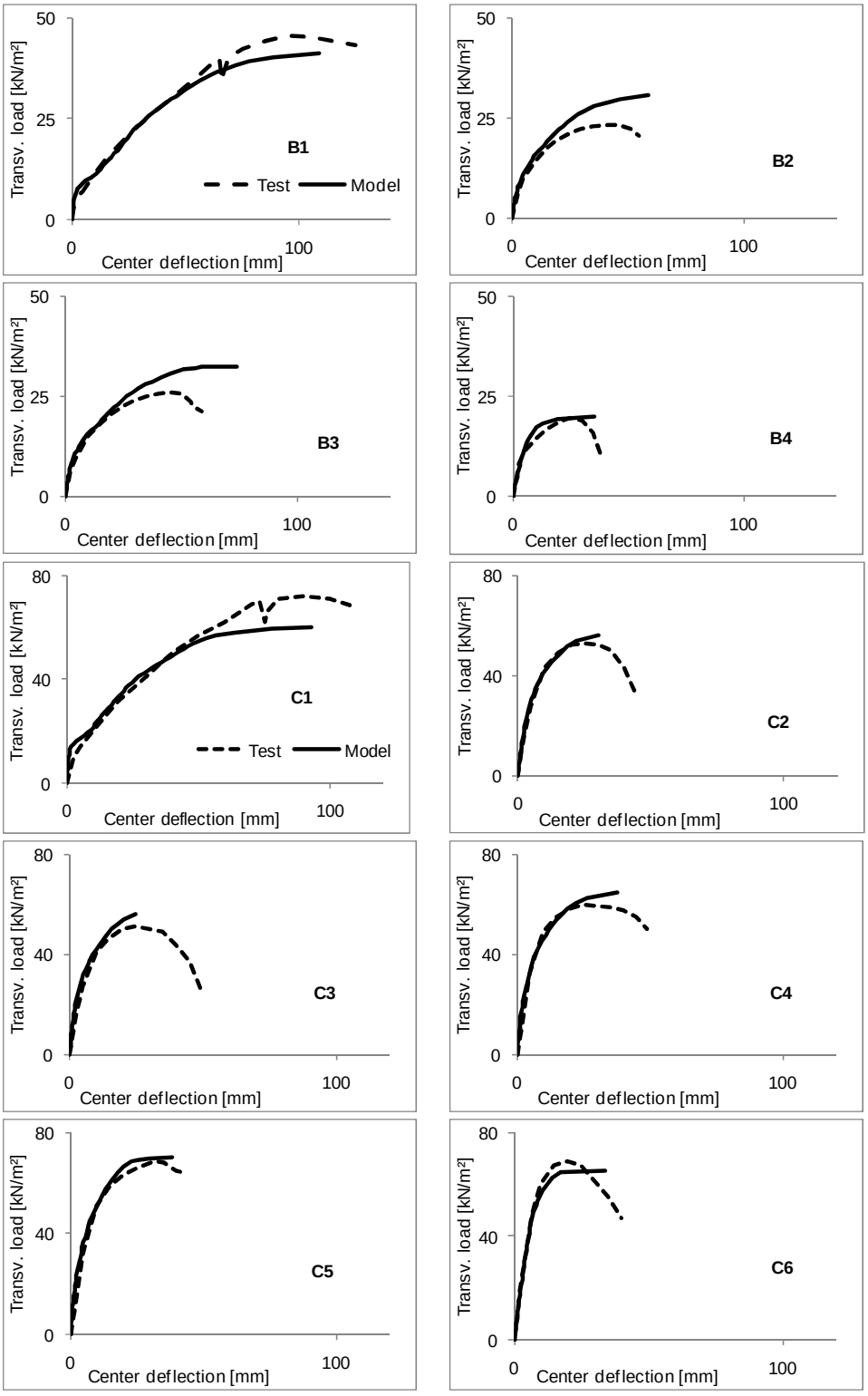

Fig. 4: The numerical results obtained with the concrete model agree with the experimental results by Ghoneim and MacGregor [26] for the different RC slabs tested.

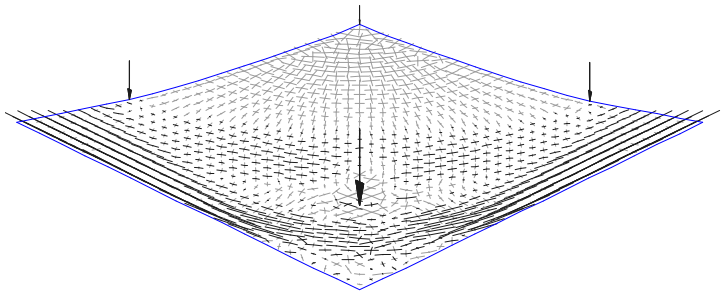

Fig. 5: Distribution of membrane forces and deformed shape for slab C1 at failure.

Fig. 5 shows the distribution and orientation of the computed principal membrane forces in a quarter of the slab C1 at failure. Compressive membrane forces are shown as black arrows whereas tensile membrane forces are represented by grey arrows. The lengths of the arrows indicate the magnitude of the membrane forces. From the deformed shape and from the distribution of forces within the shells, it can be seen that the slab develops tensile membrane action to sustain the applied load. A compressive ring develops in the concrete. In slab C1, failure eventually occurs by excessive yielding of the steel rebars; the strain in some bars exceeds 0.15 at failure.

This application shows that the model can, at a structural level, represent the transition from bending to tensile membrane action while the slab is subjected to in-plane forces. In this test, these forces have been applied as external forces while, in a fire situation, they may arise from restraint to thermal expansion.

4. Applications at high temperature

4.1 RC slab subjected to ISO fire

This example illustrates the ability of the concrete model to be used in the numerical analysis of concrete structural members in fire situations. An experimental fire test carried out at BRANZ [27] on a reinforced concrete flat slab has been simulated. The tested slab is 3.30 m wide by 4.30 m long and it is simply supported at all four edges with the edges horizontally unrestrained. The flat slab is 100 mm thick and is reinforced by 200 mm²/m steel reinforcement in each direction with a concrete cover of 25 mm. The yield strength of the steel used in the slab is 565 N/mm². The concrete that was used in the test is a normal weight concrete with siliceous aggregates. The concrete compressive strength determined by cylinder crushing test is 37 N/mm². The slab was subjected to ISO fire exposure for 3 hours while carrying a constant uniformly distributed load equal to 3.0 kN/m². The slab, which deformed into double curvature, survived the 3 hours ISO fire exposure without collapse.

The transient temperature distribution on the thickness of the shell finite elements is determined here by means of a uniaxial thermal analysis, assuming that the temperature gradient is perpendicular to the plane of the slab. Linear Conductive elements are used with temperature dependent thermal properties. At the boundaries, convection and radiation heat transfers are taken into account using the equations from Eurocode 1 Part 1-2 [28]. The thermal properties for siliceous concrete are taken from Eurocode 2. Temperatures in the slab were recorded during the test at the heated surface, at the unheated surface and at 55 mm

depth within the slab. Fig. 6 gives the comparison between the temperatures predicted by SAFIR and the measured temperatures at these locations.

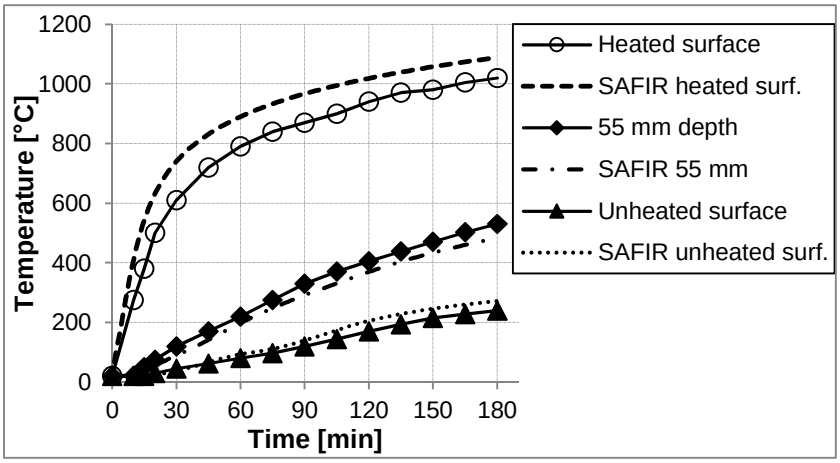

Fig. 6: Measured [27] and computed temperatures in the flat slab.

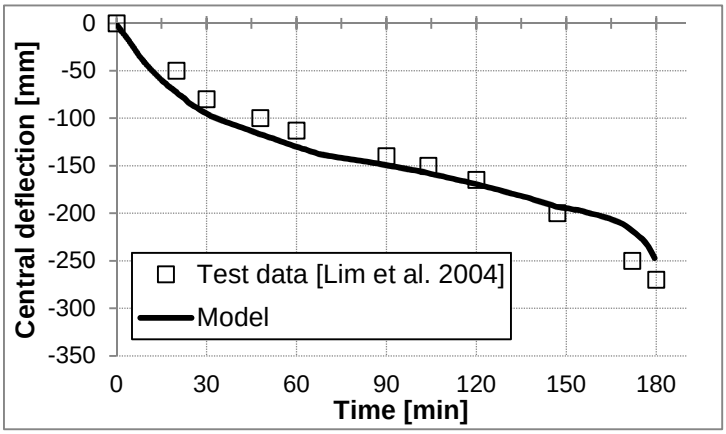

Fig. 7: Evolution of the vertical deflection with time.

Shell finite elements are used for the structural analysis. The slab is subjected to a uniformly distributed load of 5.4 kN/m² which represents the sum of the self-weight, 2.4 kN/m², and the applied load, 3.0 kN/m². This load of 5.4 kN/m² corresponds to a load ratio of approximately 0.40 for this slab. The temperature evolution in the slab is taken from the thermal analysis performed before the structural analysis. The concrete model is used for the thermo-mechanical behavior of concrete whereas the material model for the steel reinforcement is taken from Eurocode 2. The predicted and measured vertical deflections at mid-span of the slab in fire are shown in Fig. 7. Three phases can be distinguished in the evolution of the deflection. First, a high deflection rate is observed, at the beginning of the fire and during approximately the first 30 min, due to significant thermal bowing. Then, the deflection rate decreases and remains approximately constant during almost 120 min. Finally, the deflection rate increases again in the final 30 min due to the heating of the steel rebars and the subsequent decrease in stiffness of these rebars. The results of the numerical simulation agree with the experimental results. The distribution of membrane forces in the slab and the deformed shape are typical of the tensile membrane action. Significant deflections are

observed even though no failure occurs after 3 hours fire exposure; the final deflection reaches 0.25 m, which corresponds to 1/13 of the slab shorter span.

4.2 RC wall subjected to fire on one face

The concrete model notably encompasses a new transient creep model based on an explicit formulation. In order to investigate the effect of the explicit modelling of transient creep on the structural response, concrete elements acting mainly in compression must preferably be analyzed. Analyses on reinforced concrete columns have previously shown the significance of the transient creep component and the necessity to model it explicitly in order to capture accurately the concrete stiffness in fire condition [15, 29]. However, these analyses were conducted using the uniaxial formulation of the model. In this section, reinforced concrete bearing walls are analyzed using the multi-axial concrete model.

An experimental test campaign on reinforced concrete walls subjected to fire on one side has recently been conducted at Notre Dame University, with all details available in [30]. One of these tests is simulated here. The wall specimen had a thickness of 380 mm, a height of 3.05 m and a length of 1.02 m. It was embedded at its base and free at the top. The fire was applied from the base of the specimen over a wall height of 1.52 m. The steel reinforcement consisted in 12 vertical bars of 25.4 mm diameter and transverse hoops/ties of 12.7 mm diameter at 230 mm spacing, with a measured yield strength of 435 MPa and 442 MPa, respectively. The concrete was calcareous with a compressive strength of 47.1 MPa. An axial load of 2400 kN was applied at the top of the specimen at ambient temperature. This was followed by the application of an initial transversal load of 36 kN, pushing the wall toward the furnace, using an hydraulic actuator connected 230 mm below the top at mid-length of the wall. This transversal load was then stepwise increased by 22 kN at 2-hour intervals during the course of the fire. The fire followed the ASTM E119 standard time-temperature curve.

The results of the thermal analysis are compared with the measured average internal temperatures of the wall at about 25 mm from the heated face and 25 mm from the unheated face, see Fig. 8. The comparison is not good for the heated face; however, the authors of the test have reported that the measurements for this specimen were questionable and that the thermocouples might have shifted away from the heated surface during concrete casting. They have also reported the measurements for another specimen, with similar conditions of furnace temperature and wall thickness. These measurements are more in line with the numerical results; they are labelled as “specimen 0” in Fig. 8.

The mechanical analysis was conducted using shell finite elements for the wall. The transversal displacement of the wall at 2794 mm height and the axial (vertical) displacement at 1778 mm height are plotted and compared to measured values in Fig. 9. The thermal gradient within the wall leads to bowing in the direction opposite to the furnace. Yet, the transversal load applied at the top of the wall pushes the wall toward the furnace. During the first 8 hours of the test, the effect of the thermal gradient prevails and the resulting transversal displacement is in the direction opposite to the furnace. The curvature reversal occurs after 8 hours of fire exposure, following the additional increase in transversal load at that time. This curvature reversal is well captured by the model. After that, the computed displacement increases dramatically, resulting in the collapse of the wall after 8 hours and 50 minutes. The test also showed an increased rate of transversal displacement after the curvature reversal, but

no collapse occurred. The test was stopped after 10 hours and 12 minutes; at that time the maximum measured transversal displacement was equal to 46 mm. The measured and computed axial displacements reasonably agree, although the simulation underestimates the axial expansion. One possible reason for this underestimation is the fact that the part of the wall located above the furnace was subjected to elevated exhaust temperature from an opening at the top of the furnace. This effect is not represented in the numerical simulation, however it is reasonable to consider that it would lead to additional thermal expansion.

An interesting feature of this test was the stepwise incremental procedure for the transversal load, because it gives an indication about the evolution of the wall bending stiffness with temperature increase. Indeed, each transversal load increment resulted in a nearly instantaneous displacement of the wall toward the furnace, the magnitude of which is dependent of the duration of fire exposure and its effect on the wall stiffness. Hence, it is interesting to compare the measured and computed value of the instantaneous displacement increase, see Table 3. This comparison gives an indication on the accuracy of the concrete model for capturing the stiffness degradation with temperature. In particular, proper evaluation of the high temperature stiffness requires necessarily an explicit computation of the transient creep. Indeed, implicit formulations do not take into account the stress-temperature history in the material, so that a sudden increase in applied compressive stress at high temperature results erroneously in a sudden increase of transient creep [15]. In the present analysis, the comparison of instantaneous displacements shows that the wall bending stiffness is reasonably captured by the concrete model. It would have been interesting to present comparison against a similar simulation conducted with an implicit transient creep model; however, no appropriate concrete model was available to conduct this analysis. The former elasto-plastic concrete model available in SAFIR was used in an attempt to perform such a comparison but the analysis stopped prematurely due to numerical convergence issues, making the comparison impossible. Besides, different concrete models would not only differ on the transient creep component but would generally include several different features, which makes it very difficult to isolate the effects of transient creep only in a comparative analysis.

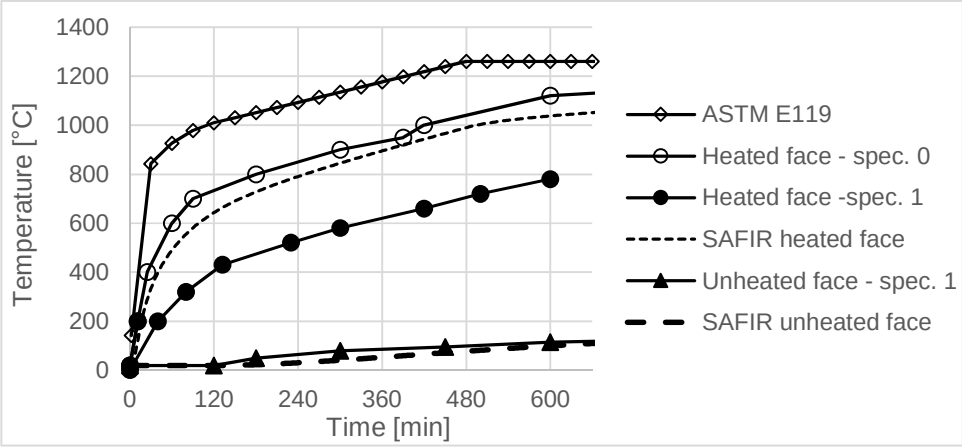

Fig. 8: Comparison between measured and computed temperatures in the RC wall.

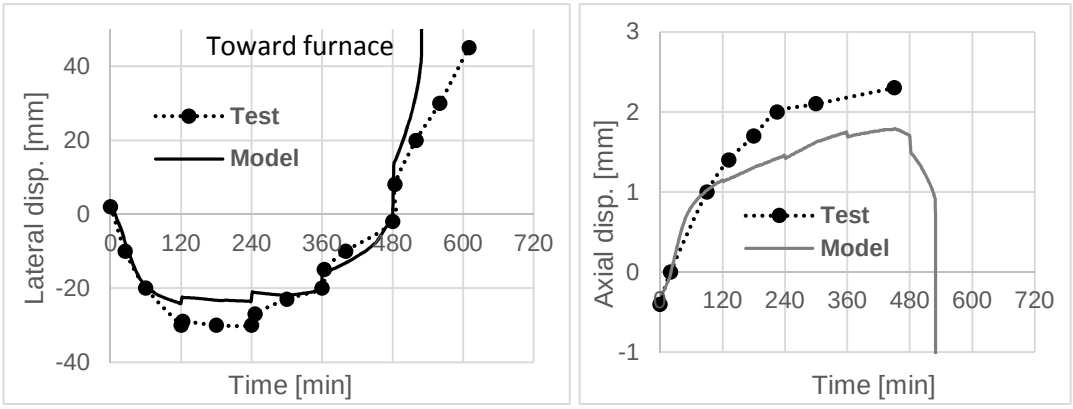

Fig. 9: Evolution of transversal displacement (left) and axial displacement (right) in the RC wall subjected to fire on one face.

Table 3: Increase in transversal displacement resulting from the stepwise load increments

Time [min]	**Transversal disp. increase [mm]**	
	Test	Model
120	0.9	1.7
240	3.0	2.6
360	4.3	4.7
480	9.4	14.2

4.3 Ulster large-scale fire test

A full-scale fire test was conducted in 2010 on a steel-concrete composite floor in the framework of a project funded by the Research Fund for Coal and Steel, in which six partners were involved [31]. The objective of the test was to investigate the development of tensile membrane action in a large composite structure in which the unprotected steel beams in the central part of the floor are made of cellular beams.

The full-scale composite floor was made of cellular steel beams connected to a composite slab. The compartment covered an area of 15 m by 9 m with a floor to ceiling distance of 3 m. The surrounding walls of the compartment were made of normal weight concrete block works with three 3 x 1.5 m openings in the front wall. All the columns and solid beams on the opening side were protected using 20 mm thick fiber boards. The surrounding cellular beams were also protected using ceramic fibers, but the two central secondary beams were left unprotected. The slab was made of 51 mm deep profile of the Kingspan Multideck 50 type with a concrete cover of 69 mm on the profile. A steel mesh of 10 mm with a spacing of 200 mm in each direction made of S500 steel was used as reinforcement. It was located at a vertical distance of 40 mm above the steel sheets. The steel profiles were made of 355 N/mm² yield strength steel, whereas the siliceous concrete used for the slab had a compressive strength of 45 N/mm². The slab was fixed on all steel beams by means of steel studs welded on the upper flanges (full connection). The structure was tested under a wood crib fire. The fire load of 700 MJ/m² was achieved using 45 standard (1m x 1m x 0.5m high) wood cribs positioned evenly around the compartment, yielding a fire load of

40 kg of wood per square meter of ground area. During the fire, the slab was carrying an applied mechanical load of 3.25 kN/m^2 plus dead weight.

The test has been entirely simulated by numerical analysis, from the computation of the gas temperature evolution in the compartment to the thermo-mechanical response of the structure. The objective was to evaluate the ability of the concrete model to be used for predictive calculations of full scale fire tests. The temperature evolution in the compartment has first been assessed by numerical simulation and the computed gas temperatures have then been used as input data for the SAFIR thermal analysis. The computation of the temperature evolution in the compartment was done using the software OZone [32, 33]. This software calculates the evolution of the gas temperature in a compartment under fire based on the combined use of a two- and a one-zone model. Comparison between computed and measured temperatures in the compartment showed rather good agreement, see Fig. 10. The measured temperatures have been taken in the four corners and in the middle of the compartment, with the openings side of the building referred to as the front side. Consequently, the temperatures computed with OZone can reasonably be used for analysis of the test, even though the temperatures observed during the test have a complex three dimensional distribution due to the geometry and ventilation conditions that OZone cannot capture. Modeling of these three dimensional temperature distributions would require the use of more advanced numerical strategies such as computational fluid dynamics; this, however, is out of the scope of this work. The temperature evolutions in the beams and in the slab sections have been determined by 2D non-linear transient thermal analyses. For the steel beams, the material properties were taken from Eurocode 3 [34] considering a convection coefficient on hot surfaces of 35.0 W/m²K, as recommended for natural fire situation. For the concrete slab, siliceous concrete following the material law of Eurocode 2 [13] has been adopted. Following the method of Eurocode 4 [35], an effective thickness of the composite concrete slab based on corrugated steel sheets is calculated for the thermal analysis; it is equal to 110 mm. The predicted versus measured temperatures within the slab are plotted in Fig. 11. The measured temperatures have been taken in the back part of the compartment, i.e. on the opposite side to the openings. The comparison shows good agreement within the slab depth for the flat part of the composite deck, i.e. between two flutes (measures B1 to B5). However, due to the use of an effective thickness model with uniaxial heat transfer, the locally higher temperature in the region just above the flutes (measures A3 and A4) cannot be captured by this simplified model. It can be seen that the temperature of the steel mesh, which is approximately located at the depth of A4-B4 measures, does not exceed 300°C during the fire.

The structural model built for the analysis of the mechanical behavior of the structure uses beam elements for the steel profiles. Local buckling and distortion of the beams can thus not be captured by the model. For the unprotected cellular beams, it was expected that web post buckling would occur at a temperature around 550-600 °C, preventing the bottom tee of the beams from playing any structural function beyond this temperature. Therefore, a fictitious material has been used for modeling the bottom tee of the unprotected beams; this material follows the laws of Eurocode 3 until 500°C and then its structural properties are linearly reduced to zero between 500°C and 600°C. This simplified approach allows considering the effect of steel web post buckling without using shell finite elements for the steel beams, which would considerably increase the complexity of the model. Shell elements

were used for the composite slab, assuming full connection between the slab and the beams. The edge beams are simply supported at the location of the columns. The concrete model is used for the reinforced concrete shells. It was chosen to neglect the tensile strength of the concrete. This decision is based on the assumption that the structure is cracked at the time when the fire starts, due to shrinkage, to the loading and to previous history of temperature variations in the structure. Although it is not possible to assess with certainty whether it was verified everywhere in this specific structure, this assumption is in line with the design requirement of Eurocode 2 that states that the tensile strength should be ignored [13].

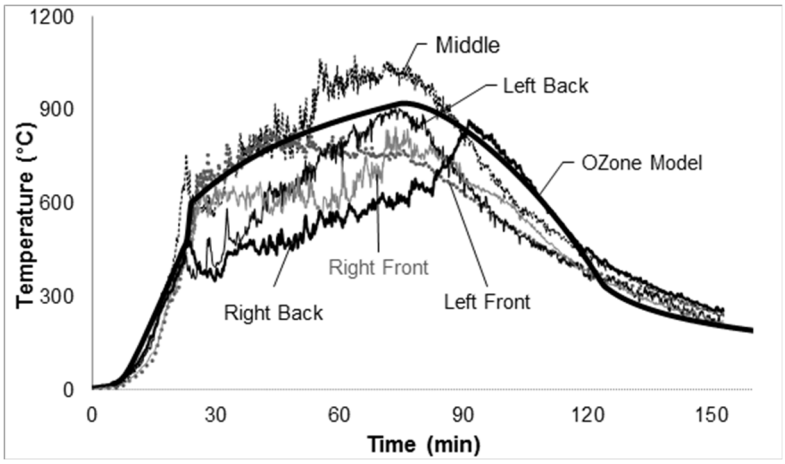

Fig. 10: Temperatures in the compartment for the Ulster test.

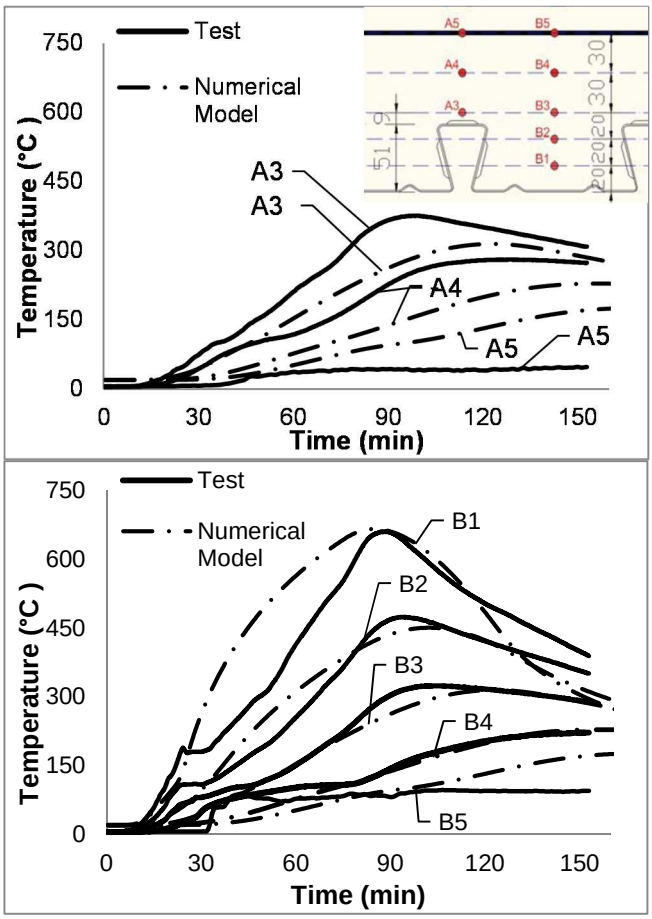

Fig. 11: Comparison of the measured versus computed temperatures within the slab.

The computed results of the vertical deflection of the floor at mid-span of the central steel beam are compared with the measured results in Fig. 12. A good correlation is obtained between the FEM model and the real behavior of the test; the numerical simulation qualitatively captures the evolution of the vertical deflection of the structure during the different phases of the natural fire. Fig. 13 shows the deformed shape and the distribution of membrane forces within the slab at ambient temperature and after 60 min fire exposure; in these figures, a different amplification factor has been used for plotting the deformed shape at ambient temperature (x20) and at high temperature (x2). The mechanism in the composite slab changes from flexural mode to tensile membrane action. After 60 min fire exposure, the unprotected steel beams have experienced web post buckling instabilities; as a result they have lost their stiffness and cannot provide support to the slab. As a consequence, the span of the slab has changed from 3.0 m to 9.0 m and membrane behavior develops within the slab.

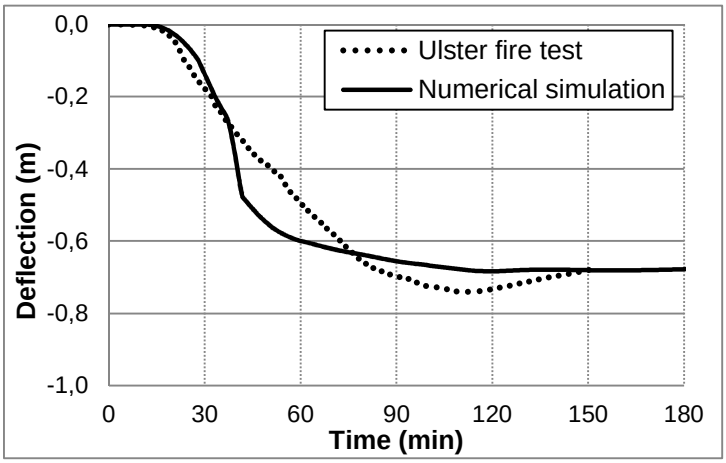

Fig. 12: Evolution of the vertical deflection of the floor at mid-span of the central steel beam.

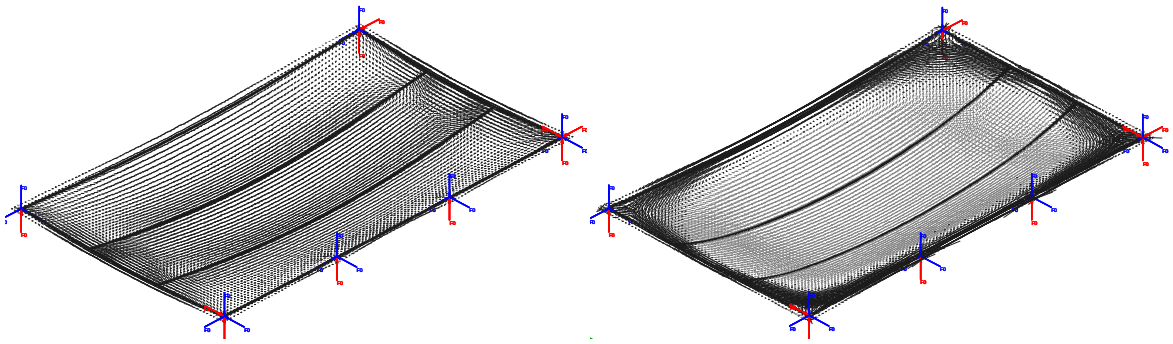

Fig. 13: Deformed shape and membrane forces at ambient (left) and high temperature (right).

The numerical simulation was able to qualitatively capture the experimental behavior of the structure subjected to natural fire. A better correspondence between the measured and computed results in Fig. 12 could probably be obtained by adapting the parameters of the model to fit with the measured values. For instance, the real temperatures measured in the sections could be used instead of the temperatures computed by a numerical thermal analysis. However, it was deliberately decided to adopt comparison conditions close to a blind simulation, without any tuning of the parameters, in order to get closer to the real conditions

met by structural engineers. Hence the obtained results give some confidence that this quite simplified model is capable of predicting the fire behavior of a large structure in fire with a satisfying level of accuracy, even though the load transfer mechanism completely changes during the course of the fire.

4.4 Fire analysis of an arch shell roof structure

In the framework of a concrete building rehabilitation, the fire resistance of a shell roof structure was studied on a request by the design office *ICB-Luxemburg*. The studied roof structure is made of two shells side by side; the span of one shell is 15.10 m and the height between the keystone and the support of the shell is 2.60 m. The length of the building is 27.00 m. The shells are made of reinforced concrete and their thickness varies from 160 mm (side) to 100 mm (center). The horizontal forces at the base of the shells are equilibrated by steel tie rods of 35 mm diameter distributed every 4.50 m. Cupolas of dimensions 1.50 m by 1.00 m are distributed in the roof every 4.50 m in the direction of their length. It was requested to analyze the fire resistance of the structure in the situation of ISO fire under one or both shells.

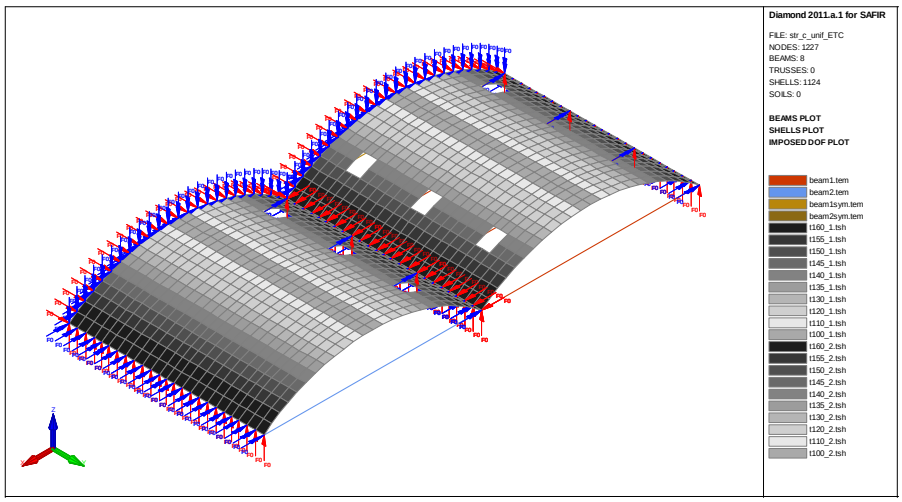

Fig.14: Finite elements model of the shell roof subjected to fire.

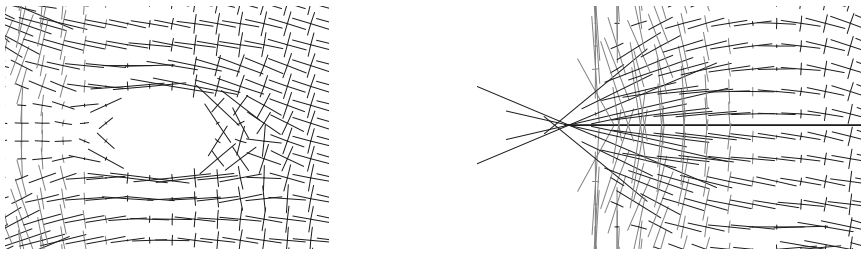

Fig.15: Membrane forces in the structure loaded at room temperature around a cupola (left) and at the anchor of a tie beam (right).

This analysis allows exploring the capabilities of the concrete model in terms of practical usefulness and numerical robustness. The structure may present different failure modes in the concrete at high temperature, such as crushing or instabilities in the shell due to restrained thermal effects, or local failure due to stress concentrations at the anchor tie

locations or around the openings. For such a complex structure, the fire response must be assessed by numerical analyses. Hence, a robust and reliable concrete model is required to be able to run the analyses until failure and gain an insight into the fire response. This example is of particular interest to demonstrate the capabilities of the model because it deals with a complex shell structure with discontinuities, stress concentrations and large displacements and because it is based on a real application of structural fire engineering.

The finite element model of the structure is shown on Fig. 14. Only half of the roof has been modeled with proper symmetry conditions imposed at the edge of the model. As the shell structure has variable thickness, 10 different sections have been used in the model with a thickness varying from 160 mm to 100 mm. The steel tie rods are modeled using beam finite elements. The concrete shell roof is reinforced in both directions by means of steel reinforcement mesh. The concrete compressive strength is 20 MPa, the reinforcement steel yield strength if 400 MPa and the tie rods yield strength is 235 MPa. In the structure, the applied loads are transmitted by the concrete shell through compressive forces toward the supports where the horizontal component is equilibrated by the effect of the steel tie rods. When loaded until failure at room temperature, the structure collapses by yielding of the steel tie rods. Fig. 15 shows the membrane forces in the structure loaded at room temperature; the concentration of the forces at the location of the steel tie rods is clearly visible.

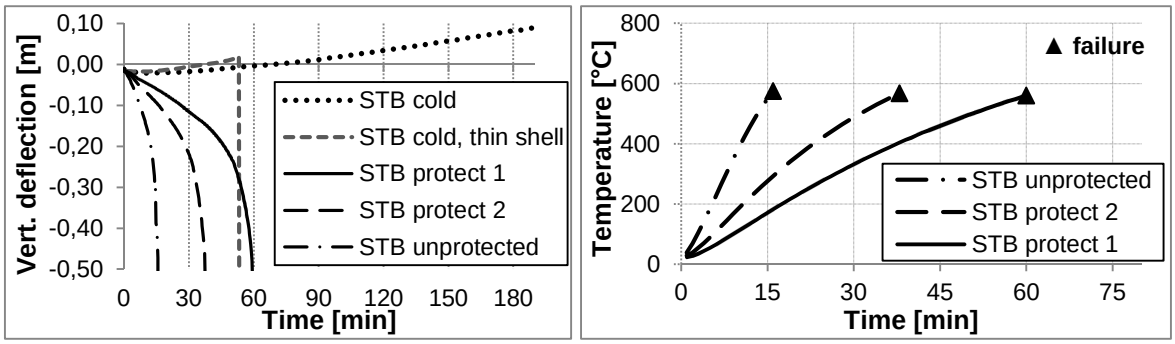

Fig. 16: Mid-span deflection of the fire-exposed shell roof as a function of the thermal protection of the steel tie beams (STB).

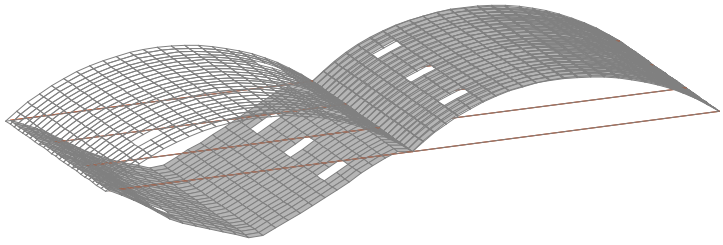

Fig. 17. Deformed shape at collapse of a concrete shell roof subjected to fire with unprotected steel tie rods.

The fire analysis of the structure is performed under self-weight loads. During the fire, the temperature increase in the steel tie rods leads to thermal expansion and decrease in stiffness and strength of these elements. As a consequence, the concrete shells lose their

horizontal supports and the structure stiffness decrease. Finally, collapse arises by a snap through of the concrete shell in the compartment where the fire develops. With thermally unprotected steel tie rods, the fire resistance of the structure is lower than 15 minutes. However, by protecting thermally the steel tie rods, the failure time can be delayed. Fig. 16 shows the evolution of the vertical displacement at the top of the heated shell roof for these different configurations. Fig. 17 shows the deformed shape at collapse in the case where the tie rods are not thermally protected. Collapse arises at a time when the temperature in the steel tie rods reaches approximately 560°C, so that the higher the thermal protection on the tie rods, the higher the fire resistance. This result may seem obvious but the numerical analysis was necessary to verify that, for a high level of thermal protection of the steel tie rods, no failure mode is reached in the concrete shell which is heated and subjected to restraint thermal forces. The structure has been analyzed in the case where the steel tie rods are perfectly protected so that their temperature remains constantly equal to 20°C during the course of the fire. Fig. 16 shows that, in the latter case, collapse by excessive compression in the concrete shell is not to be feared within 180 minutes of ISO fire exposure.

The analysis has been repeated considering a thinner concrete shell, with a uniform thickness of 80 mm. The steel tie rods have been considered as perfectly protected, with a temperature constantly equal to 20°C. In this case, it was expected that a failure mode in the concrete shell would be observed when the shell is submitted to fire. The results show a fire resistance lower than 1 hour for this structure, see Fig. 16. Failure occurs in the heated concrete shell which is submitted to significant restrained thermal effects. As a conclusion, it appears that the actual concrete shell design (with a thickness varying from 100 mm to 160 mm) is appropriate to avoid any failure in the concrete during fire. The fire resistance can thus be improved simply by adding thermal protection to the steel tie rods.

5. Conclusion

A new multiaxial constitutive model for concrete at high temperature has been developed based on a plastic-damage formulation. The detailed theoretical and computational aspects of the model have been presented in a previous publication [11]. In the present paper, the concrete model has been used in numerical simulations performed with finite element software dedicated to the analysis of building structures in fire. The objective was to demonstrate the capabilities of the concrete model in a performance-based framework and to show that it can be used for practical applications in structural fire engineering.

The simulations of experimental tests on structural elements presented in this paper have highlighted the reliability and accuracy of the concrete model. In particular, the model succeeds in capturing the crack pattern in a plain concrete specimen subjected to combined shear and tensile force, and the development of tensile membrane action in reinforced concrete slabs. Moreover, the examples of Section 4.3 and 4.4 were taken from real projects, which gives some confidence about the ability of the concrete model to be used for structural fire engineering applications.

Although the proposed model is fully three-dimensional, no application using solid finite elements with a three-dimensional stress state has been presented in this paper, mainly because of the difficulty to find experimental data in the fire situation. Practical applications

based on 3D solid finite elements in the field of building structures would include, for instance, the analyses of joints, shear punching in flat slabs, or concrete filled steel tubular columns. The study of this class of problems using the new concrete model appears as an interesting perspective for future works.

REFERENCES

[1] J. Ju, On energy-based coupled elasto-plastic damage theories: constitutive modeling and computational aspects, Int. J. Solids Struct. 25 (1989) 803-833.
[2] J. Lubliner, J. Oliver, S. Oller, E. Onate, A plastic-damage model for concrete, Int. J. Solids Struct. 25 (1989) 299-326.
[3] J. Lee, G.L. Fenves, Plastic-damage model for cyclic loading of concrete structures, Journal of Engineering Mechanics ASCE 124 (1998) 892-900.
[4] W. Krätzig, R. Pölling, An elasto-plastic damage model for reinforced concrete with minimum number of material parameters, Computers and Structures 82 (2004) 1201-1215.
[5] P. Grassl, M. Jirasek, Damage-plastic model for concrete failure, Int. J. Solids Struct. 43 (2006) 7166-7196.
[6] J.Y. Wu, J. Li, R. Faria, An energy release rate-based plastic-damage model for concrete, Int. J. Solids Struct. 43 (2006) 583–612.
[7] G. Voyiadjis, Z. Taqieddin, P. Kattan, Anisotropic damage-plasticity model for concrete, International Journal of Plasticity. 24 (2008) 1946–1965.
[8] R.K. Abu Al-Rub, G.Z. Voyiadjis, Gradient-enhanced Coupled Plasticity-anisotropic Damage Model for Concrete Fracture: Computational Aspects and Applications, Int. J. Damage Mechanics. 18 (2009) 115-154.
[9] Z. Taqieddin, G.Z. Voyiadjis, ASCE F., A.H. Almasri, Formulation and verification of a concrete model with strong coupling between isotropic damage and elastoplasticity and comparison to a weak coupling model, J. Eng. Mech. A.S.C.E. 138 (2012) 530–541.
[10] W. Nechnech, F. Meftah, J.M. Reynouard, An elasto-plastic damage model for plain concrete subjected to high temperatures, Engineering Structures. 24 (2002) 597-611.
[11] T. Gernay, A. Millard, J.M. Franssen, A multiaxial constitutive model for concrete in the fire situation: Theoretical formulation, Int. J. Solids Struct. 50 (2013) 3659-3673.
[12] A. Khennane, G. Baker, Thermoplasticity Model for Concrete under Transient Temperature and Biaxial Stress, Proc. R. Soc. Lond. 439 (1992) 59-80.
[13] European Committee for Standardization. Brussels; 2004. CEN Eurocode 2 - Design of concrete structures - Part 1-2: General rules – Structural fire design.
[14] T. Gernay, J.M. Franssen, Consideration of transient creep in the Eurocode constitutive model for concrete in the fire situation. In: Kodur V, Franssen JM, editors. Proc. of the 6th Int. Conference Structures in Fire. Lancaster PA: DEStech Publications; 2010; p. 784-791.
[15] T. Gernay, J.M. Franssen, A formulation of the Eurocode 2 concrete model at elevated temperature that includes an explicit term for transient creep, Fire Safety J 51 (2012) 1-9.
[16] R. de Borst, P. Peeters, Analysis of concrete structures under thermal loading, Computer methods in applied mechanics and engineering. 77 (1989) 293-310.

[17] T. Gernay, A multiaxial constitutive model for concrete in the fire situation including transient creep and cooling down phases. Ph.D. thesis, University of Liege, 2012.
[18] Comité Euro-International du Béton-Fédération internationale du béton, 1990. CEB-FIB Model code 1990 Bulletin d'information. Lausanne, Switzerland.
[19] H.K. Hilsdorf, W. Brameshuber, Code-type formulation of fracture mechanics concepts for concrete, International Journal of Fracture. 51 (1991) 61-72.
[20] P.H. Feenstra, R. de Borst, A composite plasticity model for concrete, Int. J. Solids Struct. 33 (1996) 707-730.
[21] J.G. Rots, Computational modelling of concrete fracture. Ph. D. Delft U. of Techn; 1988.
[22] J.M. Franssen, SAFIR: A thermal/structural program for modeling structures under fire, Engineering Journal - A.I.S.C 42 (2005) 143-158.
[23] M.B. Nooru-Mohamed, Mixed-mode fracture of concrete: an experimental approach. Ph. D. thesis, Delft University of Technology; 1992.
[24] M. di Prisco, L. Ferrara, H. Meftah, J. Pamin, R. de Borst, J. Mazars, J.M. Reynouard, Mixed mode fracture in plain and reinforced concrete: some results on benchmark tests, Int. J. of Fracture 103 (2000) 127-148.
[25] R.K. Abu Al-Rub, S.M. Kim, Computational applications of a coupled plasticity-damage constitutive model for simulating plain concrete fracture, Engineering Fracture Mechanics 77 (2010) 1577–1603.
[26] M.G. Ghoneim, J.G. MacGregor, Strength and Stability of Reinforced Concrete Plates Under Combined Inplane and Lateral Loads. Structural Engineering Report No. 176. Alberta, Canada: Department of Civil Engineering, University of Alberta; 1992.
[27] L. Lim, A. Buchanan, P. Moss, J.M. Franssen, Numerical modelling of two-way reinforced concrete slabs in fire, Engineering Structures 26 (2004) 1081-1091.
[28] European Committee for Standardization. Brussels; 2002. CEN Eurocode 1 – Actions on structures - Part 1-2: General actions – Actions on structures exposed to Fire.
[29] T. Gernay, Effect of transient creep strain model on the behaviour of concrete columns subjected to heating and cooling, Fire Technology 48 (2012) 313-329.
[30] K.A. Mueller, Y.C. Kurama, M.J. McGinnis, Out-of-Plane behaviour of two reinforced concrete bearing walls under fire: A full-scale experimental investigation, ACI Structural Journal 111 (2014) 1101-1110.
[31] O. Vassart, C.G. Bailey, M. Hawes, A. Nadjai, W.I. Simms, B. Zhao, et al. Large-Scale Fire Test of Unprotected Cellular Beam Acting in Membrane Action, Proc. of the ICE: Structures and Buildings. 165 (2012) 327-334.
[32] J.F. Cadorin, J.M. Franssen, A tool to design steel elements submitted to compartment fires - OZone V2. Part 1: pre- and post-flashover compartment fire model, Fire Safety J 38 (2003) 395-427.
[33] J.F. Cadorin, D. Pintea, J.C. Dotreppe, J.M. Franssen, A tool to design steel elements submitted to compartment fires - OZone V2. Part 2: Methodology and application, Fire Safety J. 38 (2003) 429-451.
[34] European Committee for Standardization. Brussels; 2005. CEN Eurocode 3 - Design of steel structures - Part 1-2: General rules – Structural fire design.
[35] European Committee for Standardization. Brussels; 2005. CEN Eurocode 4 - Design of composite steel and concrete structures - Part 1-2: General rules – Structural fire design.